small NANO MICRO

Microfluidics

DOI: 10.1002/smll.200700641

Microfluidic Pump Powered by Self-Organizing Bacteria**

Min Jun Kim and Kenneth S. Breuer*

***R**esults are presented that demonstrate the successful use of live bacteria as mechanical actuators in microfabricated fluid systems. The flow deposition of bacteria is used to create a motile bacterial carpet that can generate local fluid motion inside a microfabricated system. By tracking the motion of tracer particles, we demonstrate that the bacterial cells that comprise the carpet self-organize, generating a collective fluid motion that can pump fluid autonomously through a microfabricated channel at speeds as high as 25 μm s^{-1}. The pumping performance of the system can also be augmented by changing the chemical environment. The addition of glucose to the working buffer raises the metabolic activity of the bacterial carpet, resulting in increased pumping performance. The performance of the bacterial pump is also shown to be strongly influenced by the global geometry of the pump, with narrower channels achieving a higher pumping velocity with a faster rise time.*

Keywords:
- biological motors
- cell motility
- metabolic activity
- microfluidics
- stimuli-responsive materials

1. Introduction

The practical development of so-called lab-on-a-chip systems for performing compact chemical analysis, DNA sequencing, and other tasks is often held up by difficulties encountered in the mechanics of mixing and pumping picoliter quantities of fluid. Candidate micro-total analysis systems (μTAS) often use either external devices, such as syringe pumps, or relatively large and inefficient integrated systems based on piezoelectric, pneumatic, electrokinetic, or electromagnetic effects.[1–3] While these approaches work, they often rely on bulky and inefficient hardware that often negates the advantages of the micrometer-scale chemical system which they support. One potentially attractive solution to this problem is to use the nanometer-scale motors from biological systems. This concept has been demonstrated in a variety of systems, such as using the F_1-ATPase rotary motor to turn a nanorod,[4,5] moving microtubules along patterned tracks of kinesin molecules,[6,7] using algae to move microspheres,[8] and finally, the use of a gliding bacteria, *Mycoplasma mobile* to rotate a microfabricated rotor.[9] In all of these examples, although the potential for a useful device that marries a biomolecular motor to an engineered system has been demonstrated, no work was extracted from the system (such as fluid pumping or mechanical shaft power).

An extremely powerful biological motor is the bacterial flagellar motor found in organisms such as *Escherichia coli* or *Serratia marcescens*.[10] These bacteria are propelled through water at speeds as high as 50 μm s^{-1} by three to five helical flagella each approximately 10 μm in length and driven by a rotary motor that measures approximately 50 nm in diameter. The rotation of the flagella strongly affects the fluid environment surrounding the cell, and this flow promotes bundling of adjacent flagella[11] and generates thrust for cell motility. In addition, the activity of *E. coli* freely swimming in solution has been shown to enhance the

[*] Prof. M. J. Kim
Department of Mechanical Engineering and Mechanics
Drexel University
3141 Chestnut St, Philadelphia, PA 19104 (USA)
Fax: (+1) 215-895-2295
E-mail: mkim@coe.drexel.edu
Prof. K. S. Breuer
Division of Engineering
Brown University
182 Hope St, Providence, RI 02912 (USA)

diffusion of tracer beads[12] and of macromolecules[13,14] dissolved in the ambient buffer. If the bacterial cell bodies are affixed onto an open surface, the rotation of the free flagella can also be utilized to generate useful work. Such active surfaces, or "bacterial carpets", have been formed by blotting a polydimethylsiloxane (PDMS) film onto a swarm plate of *S. marcescens*,[15] and the bacterial carpet can also be used to transport freely floating PDMS "barges"[15] and polystyrene beads[16,17] through a fluid medium. The bacteria in the carpet metabolize a wide variety of food sources and can even maintain their motility for several hours in the absence of food.[15,18] This robustness is highly attractive for microfluidic applications.

In this Full Paper, we extend the use of bacterial carpets to demonstrate that they can be used to generate useful work in a microfluidic system. We first present results demonstrating that bacteria can be flow-deposited to form an active bacterial carpet coating the surface of an enclosed microfluidic system. The key result, however, is that we show that the system of thousands of independent bacterial cells self-organizes, resulting in a collective motion that is capable of pumping fluid through the microchannel for several hours at speeds as high as 25 μm s^{-1}. Lastly, we demonstrate the ability to affect the global performance of the bacterial pump by using both geometric variations and chemical stimuli introduced in the surrounding motility buffer.

2. Results and Discussion

2.1. Formation of Flow-Deposited Bacterial Carpets

The experiments were conducted using a microfluidic channel fabricated from polydimethylsiloxane (PDMS) using standard "soft lithography" micromolding techniques.[13,19] The nominal channel dimensions used were 15 μm (height) by 200 μm (width) by 15 mm (length) (Figure 1). Since the microchannel is fully enclosed, we cannot form bacterial carpets using the blotting technique.[15] Instead, bacterial carpets were formed on the inner surfaces of the microfluidic channel using a novel flow-deposition procedure in which bacteria (*S. marcescens*) are pumped slowly into the microchannel and allowed to adhere by natural accretion. As the bacteria flow into the channel, they collide and adhere to the PDMS and glass surfaces. The density of the bacterial carpet and the orientation of the cells were observed (using differential interference contrast (DIC) microscopy) during the carpet-deposition process (Figure 2). The

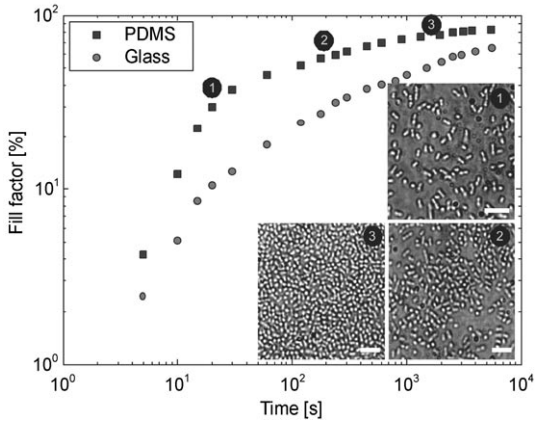

Figure 2. Coverage versus time of *S. marcescens* on PDMS and glass surfaces inside a microchannel. The test geometry is a microchannel measuring 15 μm deep, 200 μm wide, and 15 mm long. Images are acquired midway down the channel axis. The carpet is created by repeatedly flowing in fresh bacteria and then letting them adhere to the surface by random accretion. Scale bars are 5 μm.

images indicate that the surface coverage increases monotonically with time, although unlike the smooth and densely packed carpets formed on an open slide by blotting from a swarm plate,[15] the flow-deposited carpet asymptotes very slowly towards 100% coverage. There are two possible causes for this apparently self-limiting behavior. Firstly, the negative charge of the cells might serve to inhibit cells from sticking in regions of existing high-density surface coverage. Secondly, the cells may generate chemical signals at high packing densities, which actively deter further accretion. Note that the PDMS surface coats more quickly than the glass surface, consistent with the fact that *S. marcescens* bacteria are known to adhere more easily to PDMS than to glass. Approximately 80% of the cells adhere to the surface as a single isolated cell, while the remainder were in contact with, or partially on top of, another bacterial cell. The Serratia marcescens cell bodies are elongated spheroids (approximately 2 μm in length, 1 μm in width). Because of the alignment by the flow that delivers them to the microchannel, the cells tend to adhere with a clear orientational preference, with about 55% of the cells aligned to within 30° of the channel's *x*-axis. After 50 min, the fill factor was measured to be 83% (±1.2%) and the average density of bacteria was 31.3/100 μm^2 (±2.1). Although a few cells were observed to stick to the surface by their flagella (tethered bacteria),[20] most of the cells stuck to the surface by their bodies with several flagella free to rotate in the flow.

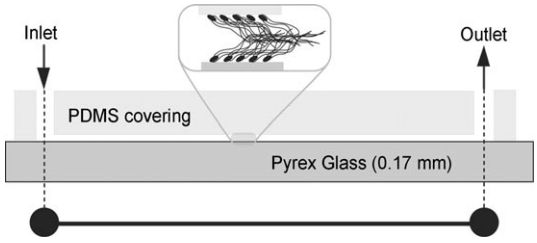

Figure 1. Schematic of bacterial-pump geometry. The flow channel is defined from below by the glass coverslip and on the sides and top by the PDMS covering. The channel dimensions are 15 μm (high) by 200 μm (wide) by 15 mm (long). The insert illustrates the bacterial carpet, which covers the entire length of the channel. The cell bodies and flagellar length are shown in approximate proportion to the channel-wall separation. However, in reality, the flagellum thickness is much smaller than shown.

NANO MICRO small

2.2. The Spontaneous Emergence of Pumping

Previous work has shown that the activity of the bacterial carpet in a sealed microfluidic channel can enhance mixing.[16] However, in the present case, the channel is not sealed at its ends, and we observe that the bacterial carpet spontaneously self-organizes and pumps fluid through the channel. Following the formation of the carpet, the external flow was switched off and the inlet and outlet tubes removed from any external pressure bias. Care was taken to ensure that the inlet and outlet tubes were at the same level (so that there were no hydrostatic pressure gradients), that there were no bubbles, and that the menisci at the ends of the inlet and outlet tubes were identical (so that there were no capillary effects). Velocity measurements were made at a fixed point at the midpoint of the channel using particle tracking velocimetry (PTV), sampling several times following the formation of the carpet (defined as $t = 0$). The average streamwise velocity through the microchannel was observed to build over the course of several minutes (Figure 3), reaching a peak velocity of approximately

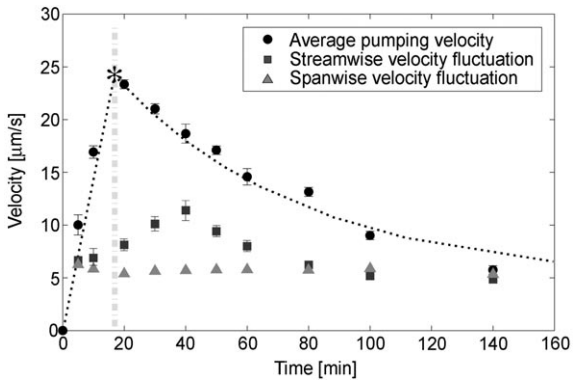

Figure 3. Evolution of the average and fluctuating velocities (in both the streamwise and spanwise directions) in the microchannel as a function of the time following the creation of the carpet-coated microchannel. The average velocity reaches its maximum at approximately $t = 20$ min, which is close to the maximum in the anisotropy of the velocity fluctuations. Even as the average pumping velocity declines, the fluctuations remain above the velocity measured by the PTV analysis because of Brownian diffusion "velocity" (4.9 μm s^{-1} for water at this temperature and Δt).

23 μm s^{-1} at 20 min after the carpet formation ($t = t^*$). At later times, the average velocity decays slowly, falling to 5 μm s^{-1} by $t = 150$ min. The velocity was observed to be uniform throughout the channel (both across the channel width *and* between the upper to the lower wall), characteristic of a plug-like flow (similar to electro-osmotic pumping and pressure-driven flow in the Hele–Shaw geometric microchannel[21–23]). To confirm that a net pumping thrust was developed only because of the suspended bacterial carpet, the experiment was repeated numerous times under different conditions. Furthermore, it was confirmed that the pumping activity could be stopped by introducing carbonyl-cyanide-*p*-trifluoromethoxyphenyl-hydrazone (FCCP, which inhibits the bacterial motor rotation) into the buffer solution. Curiously, the tracer particles were always observed to move in the same direction, suggesting that the "seed" that initiates the pumping is related to the carpet fabrication sequence, although the reasons for this are not clear.

The general history presented in Figure 3 was observed in all our experiments, and we can parameterize the behavior as comprised of two phases: a period of rapid growth, which can be characterized as a linear rise:

$$U = \alpha t (t < t^*) \tag{1}$$

where α is the growth rate, followed by a period of exponential decay:

$$U \propto e^{-\beta t} (t > t^*) \tag{2}$$

where β is the decay rate.

The physical mechanisms that lead to the observed bulk pumping of fluid are difficult to confirm directly. However, the statistics of the tracer particle motion do lead to several insights. Brownian motion of the tracer particles appears in the PTV analysis as a "diffusion velocity",[24] resulting from particle dispersion during the sampling time. The diffusion velocity is characterized by zero mean, random orientation, and a standard deviation (for the experimental conditions tested), σ, of 4.9 μm s^{-1}. The measured particle velocity distributions show this character after long times when the bacteria have all de-energized, although during the period when the carpet is actively pumping, the velocity fluctuations are observed to be significantly higher than this baseline. The velocity fluctuations are also highly anisotropic, with the fluctuations in the streamwise direction, x, as much as three times larger than the fluctuations in the cross-stream direction, y (Figure 3). The overall pumping performance peaks well before the streamwise velocity fluctuations reach their maximum. After reaching a maximum, the pumping velocity decays approximately exponentially, although the anisotropy in the velocity fluctuations lags somewhat, not reaching its maximum until about 40 min after the carpet formation. The velocity fluctuations become isotropic after about 80 min although they remain higher than what would be expected for purely Brownian motion, suggesting that the bacteria still exhibit some motile activity but are unable to coordinate sufficiently to sustain any significant pumping. Several hours later, after the bacteria have de-energized, the pumping motion was no longer observed, and the diffusion velocities were found to be close to that predicted by Brownian motion.

2.3. Effects of Glucose Concentration

The performance of the pump can be controlled by adding glucose (a food source for the bacteria) to the buffer solution. Although the time at which the maximum velocity is achieved (t^*) does not change, an increase in the buffer glucose concentration results in a rise in U_{max} (and thus an increase in the growth rate, α) as well as a decrease in the

decay rate, β (Figure 4). Although *S. marcescens* are able to maintain motility for long periods of time relying solely on an endogenous energy reserve, in the presence of glucose

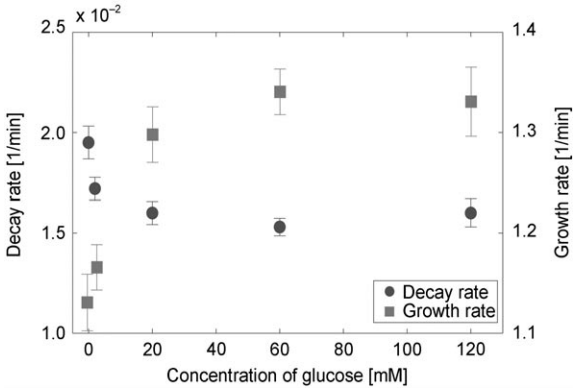

Figure 4. Variation of the growth and decays rates of the pumping velocity as a function of glucose concentration (0, 2, 20, 60, and 120 mM). Although the pump rise time does not change, the addition of glucose dose result in higher maximum pumping speeds (due to higher metabolic activity of the bacteria) and longer-lived pump operation (presumably due to improved transport of buffer).

their metabolic rate (and oxygen consumption) increases dramatically, resulting in higher motor rotation rates.[18,25] The glucose consumption rate per cell saturates such that additional increases yield no further increased motor performance, and this is the likely explanation for the observed plateau in the pump behavior at higher glucose concentrations.

The reduction in the pumping velocity decay rate (β) indicates an extended lifetime with the addition of glucose, a result in direct contrast to the behavior of bacterial carpets in sealed (nonpumping) systems,[16] in which case the carpet activity decays *faster* as glucose concentration increases. In the sealed system, the reduced performance is a result of the much faster consumption of dissolved oxygen (which cannot be replenished in a sealed system) as well as the faster poisoning of the motility buffer by the catabolic products of the bacterial carpet, which lead to a drop in the buffer pH, and hence a reduced motor effectiveness. However, in the open system considered here, the increased pumping velocity results in more fresh buffer (with fresh dissolved oxygen) being introduced to the carpet and a faster removal of the acidic waste products of the carpet's catabolism. Thus, the heightened activity of the carpet not only improves the performance of the pump but also serves to maintain the local pH, and to maintain a healthy environment for a longer time, thus, extending the carpet's working lifetime.

2.4. Effects of Pump Geometry

While the carpet rise time, t^*, was not affected by the glucose concentration, it was found to be a strong function of the channel geometry. The geometry of the microchannel may affect the performance of the bacterial pump in two ways. Firstly, it is known that the behavior and motion of bacteria can be influenced by their geometric environment.[26,27] Secondly, even if the bacterial behavior remains unchanged, the self-organization of the carpet may be a function of the pump geometry.[16] The results shown thus far were performed in a microchannel measuring 15 μm deep, 200 μm wide, and 15 mm long. Five channels were tested with widths, w = 50, 100, 200, 400, and 800 μm (keeping the length and depth constant). For each geometry, the maximum velocity, U_{max}, and the rise time, t^*, were measured. The results are quite striking (Figure 5), showing that the maximum pumping velocity achieved and the time to peak performance are strongly affected by the channel width. The optimal performance is achieved in the 50 μm wide channel, which achieved a maximum pumping velocity of 25 μm s^{-1}, and was reached almost immediately after the channel is created. In contrast, the widest channel tested, w = 800 μm, barely pumps at all, and requires over 25 min to reach its peak performance. Decreasing the pump length also increased the maximum pumping speed and decreased t^*; however, in this case, the effects were quite modest (improvements of approximately 10% for a threefold reduction in channel length).

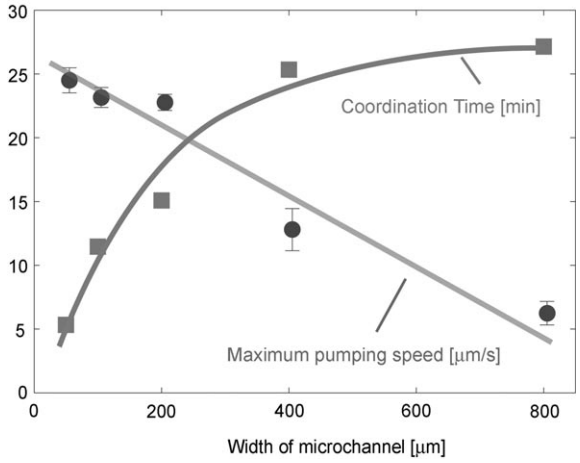

Figure 5. Dependence of the maximum pumping velocity, U_{max}, and the pumping rise time, t^*, on the channel width. The narrow channels coordinate faster and achieve higher maximum velocities than wider channels.

3. Discussion

The results presented demonstrate clearly that the collective motion of thousands of bacterial flagella gives rise to net fluid motion through the microfabricated channel. In explaining these observations, we hypothesize that the pumping results from the rise of a global coordination in the flagellar orientation throughout the channel. The flagellar motor rotates predominantly counterclockwise, punctuated by random intervals of clockwise rotation.[28,29] Since the control of the sense of rotation for each flagellar motor is

NANO MICRO small

independent of its neighbor (even within the same cell), it seems unlikely that the clockwise and counterclockwise rotations become coordinated across the carpet. However, hydrodynamic interactions between closely spaced rotating flagella do lead to coordination and the formation of flagella bundles,[11] and in a carpet of densely packed cells, the interactions between many flagella in a neighborhood leads to the formation of local pockets of coordinated fluid motion. Such areas of organization were observed in the bacterial carpet formed on open surfaces[15] in the form of coherent "rivers", along which fluorescent beads were transported at speeds as high as 60 μm s^{-1}, and "whirlpools", in which the beads were observed to move in a large-scale (15–20 μm) vortical motion. In the microchannel flow considered here, since the fluid is constrained to flow predominantly in one direction, a coherent river arising at one point in the channel will act to preferentially force the fluid in the same direction throughout the entire channel. This flow will entrain other flagella along the same direction and thus provide a positive feedback mechanism, which might serve to assist in the growth of these coordinated regions, analogous to the growth of crystal domains during solidification. In this manner, larger areas of coordinated pumping motion are established, and the average pumping speed rises.

The evolution of the spatial correlation function supports this explanation. Figure 6 shows the normalized spatial correlation function of velocities in the bacterial pump, measured at four distinct times. Immediately after the formation of the carpet (Figure 6a), the correlation function has well-defined peaks and valleys, representing a typical vortex spacing of approximately 15 μm. However, unlike the open-carpet results of Darnton et al.,[15] the correlation of the carpet confined to the channel continues to increase and by $t = 20$ min, at the height of the pumping (Figure 6b), the peak–valley structure in the correlation function has completely disappeared, replaced by a uniformly high correlation that maintains a relatively constant value over the entire field of view (40 μm). This uniformity in the correlation function is obviously associated by the high correlation associated with the uniform pumping flow. As time progresses, the pumping decays (Figure 6c) and the peak–valley structure reappears, this time with a larger typical vortex size, suggesting that the global coordination that was established has started to break down into smaller domains ("whirlpools"). After long times (Figure 6d), the nonmotile carpet shows no correlation beyond a length scale of approximately 10 μm (which is approximately the length of the flagella, now floating passively in the buffer but presumably still imposing some organization via their inactive presence). This behavior is also reflected in the integral of the correlation function, which defines a correlation length scale, l^*. This was computed and was observed to have behavior that closely tracks the mean pumping speed (Figure 3), reaching a maximum value of 12 μm at $t = 25$ min before falling slowly, approaching a value of 2.5 μm after long times.

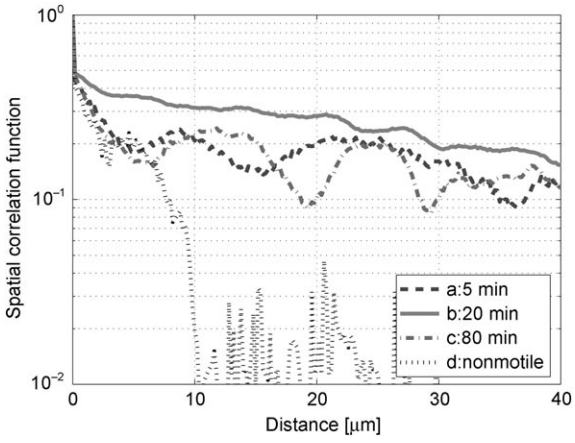

Figure 6. Evolution of the normalized spatial correlations between measured fluid velocities as a function of the distance and time between them. Four phases of the pump operation are shown: a) 5 min (shortly after carpet formation), b) 20 min (at the height of pump operation), c) 80 min (after pumping activity has declined), and finally d) for a nonmotile carpet.

The strong dependence of the pump rise time, t^*, and the pumping speed, U_{max}, on the channel width also supports this view of the underlying coordination mechanics. The onset of global pumping requires that the size of the coordinate fluid river becomes comparable to the channel width. Rivers of smaller dimension will not have sufficient "authority" to establish a net fluid flow. Thus, wider channels result in degraded pumping performance in two ways: firstly, it takes longer for the coordinated fluid region to grow to the critical size, and, secondly, larger regions will encompass more counterproductive fluid motion, and hence exhibit lower net pumping velocities.

The reason for the decay in the pump's effectiveness over time is not obvious. The bacteria were grown aerobically and with nutrients and thus require oxygen and nourishment to maintain motility. Taking into account an oxygen consumption rate per cell and neglecting fresh oxygen brought in by the pumping of fresh buffer solution,[24,30] we can estimate that the bacteria in the carpet would require over 40 h to consume all of the available dissolved oxygen. Since the duration of a typical experiment is less than 3 h, it seems reasonable to conclude that the observed decline in the pumping behavior is not primarily due to a global oxygen deficiency. However, recalling the differences between the present system and the closed carpet, which shows a faster decline in health,[16] it seems like oxygen replenishment and/or waste-product removal does have an influence on the carpet's health and this may be related to the adhesion of the cells to the surface and thus their inability to sample new (fresh) regions of the buffer solution.[31] The cells' lack of motility coupled with their high packing density may result in a locally nutrient-poor environment that contributes to their premature loss of robust motile behavior.

4. Conclusions

The formation of active surfaces inside engineered microfluidic networks, and the subsequent demonstration of

biologically powered mixers and pumping systems is, we believe, an important first step in the integration of biomolecular motors with engineered systems and in the development of autonomous microfluidic systems. The performance of microfluidic devices powered by bacterial carpets has been shown to be a sensitive function of both the environment in which the bacteria live as well as the global device geometry. Factors that enhance bacterial motility, such as the concentration of glucose (and, not shown in the present paper, the temperature of the system), similarly affect the carpet motility and hence the overall transport.

The rise of the pumping appears to be due to the onset of a self-organized global coordination amongst the flagella that form the bacterial carpet. Once the carpet is formed on the inner walls of the microchannel, the cells on the carpet immediately begin to self-coordinate their flagellar motion, most likely due to the hydrodynamic interaction between the flagella. Hence, even though the bacterial pump is at the initial state (5 min after formation), the average pumping velocity reaches approximately $10\,\mu m\,s^{-1}$. Some additional time, usually approximately 10 min, is apparently required before the collective activity of the flagella reaches its maximum efficiency with the flow optimally aligned along the major axis of the channel. At that point, the flow rate reaches about $25\,\mu m\,s^{-1}$ (approximately 60% of the cell's smooth swimming velocity). The spatial correlation data suggests that, in the early stages of the carpet's formation, vortices and streams form spontaneously but that this motion initially has no global consequences because fluid elements are simply pushed around at random. However, unlike the flow over an open bacterial carpet, these coherent motions are constrained in the cross-stream direction and so the fluid path is directed preferentially along the axis of the channel. This directionality is self-reinforcing and entrains surrounding flagella, growing until a critical size of coordinated motion is established, which allows for sustained fluid pumping. This conceptual model is supported by the acceleration in the onset of pumping that is observed as the channel width is reduced. In order for net pumping to become viable, the size of the coordinated domain must be comparable with the width of the channel, and clearly this will happen faster in smaller channels.

The global coordination does not last, and the average pumping velocity decays after about one hour of operation although the reasons for this are still unclear. We see the breakdown of this global structure into discrete coherent domains, as evidenced by the reappearance of peaks in the spatial correlation function. Even though the cells appear to maintain some level of motility, the decline of the pump may be associated with the generation of a low-nutrient (or high-waste-product) environment, which cannot be refreshed sufficiently fast to compensate for the high metabolic activity in the immediate vicinity of the carpet.

Beyond any scientific importance, these results also define an opportunity to use *biological organisms as mechanical actuators* in engineered systems. Bacteria are exquisitely sensitive to a wide variety of external stimuli. They respond to thermal and chemical gradients that directly influence their motility characteristics and form the basis for chemotactic and thermotactic responses.[32] Changes in factors such as temperature, the concentration of certain sugars, or the spatial environment can stimulate the bacteria's sensory pathway and affect aspects of their motor performance, including the rotation direction, duty cycle, and frequency.[33–35] Given this sensitivity, it seems quite feasible that one can find, or engineer (by genetic modification), organisms that can respond to specific stimuli and, through this means, control and regulate the operation of a bacterial pump and build a wide variety of systems of practical relevance. As a matter of fact, the phototactic response of bacteria to UV light[36] may be utilized to exert on/off control of the pump immediately. Of course, using living cells as fluidic actuator is not without challenges: the cells metabolic products might be a contamination source to the primary fluid, and the issues of motility and device longevity present substantial challenges. Nevertheless, the approach described here may prove useful as these issues are addressed.

5. Experimental Section

Cell preparations: *S. marcescens* (ATCC 274, American Type Culture Collection, Manassas, VA) used in this study were provided by Linda Turner and Howard Berg of the Rowland Institute at Harvard University. For the best motility, the 100 μL frozen aliquot of *S. marcescens* was suspended in 10 mL of Luria Bertani (LB) growth medium and incubated for 3–4 h at 30–34°C. The cultures were aerated by gently shaking the tube at about 180 rpm. The bacteria were removed from the incubator during the exponential phase of their growth and separated from the nutrient broth, by centrifugation at 2200 *g* for 10 min (3000 rpm). After centrifugation, the resulting pellet was soft and not too tightly packed. The supernatant was poured off and the cells were gently resuspended in 0.5 mL of buffer. Buffer (pH 7, comprising 0.01 M KPO_4, 0.067 M NaCl, and 10^{-4} M ethylenediaminetetraacetic acid) was then added to bring the total volume to 10 mL. This separation process was repeated three times to ensure that all the growth medium was removed.

Flow-deposited carpet formation: To flow-deposit a bacterial carpet, buffer solution containing a high concentration (2×10^9–$5\times10^9\,mL^{-1}$) of motile *S. marcescens* was pumped through the channel at a low flow rate ($0.05\,\mu L\,min^{-1}$) from right to left (Figure 1). After 5 s, the pump was switched off, and the system was allowed to settle for 5 min. During this time, the bacteria swim randomly through the channel, sticking on contact to bare spots on the PDMS surface. The flow-and-settle cycle was repeated 10 times until the surface was coated to the desired fill factor of 75–85%. During the settling time, the system was rotated to ensure an even coating of all surfaces. During carpet formation, the cell adhesion was monitored by using a 100× oil-immersion objective and DIC microscopy (Nikon TE-200 inverted microscope, 100× oil-immersion lens). After the adhesion phase, the channel was rinsed with clean motile buffer, introduced

NANO MICRO small

from left to right. Finally, the tracer particles were introduced in a buffer solution that was pumped from right to left. In this way the left and right ports of the channel were alternately used as inlets to purge the channel of the fluid from previous injections. To eliminate the possibility of apparent pumping caused by a pressure bias, the external flow was switched off and the inlet and outlet of the channel were maintained at equal pressure for several minutes. This period also allowed the system to purge the influence of any previously imposed flows during carpet formation (injection of buffer and tracer particle solution). Pumping was observed to arise after this settling period.

Velocity measurements: Following the formation of the bacterial carpet, the channel was flushed with fresh buffer for 10 min. Following this, a solution of motility buffer seeded (0.05% by volume) with 490-nm fluorescent beads ($\lambda_{ex} = 520$ nm, $\lambda_{em} = 612$ nm; Duke Scientific, Palo Alto, CA) was introduced (0.2 μL min^{-1}). The filling tubes (which were the same diameter, thus, eliminating the possibility of surface-tension-induced flow) were disconnected from the syringe pump and carefully arranged with their menisci at the same height (so as to prevent any spurious flow through the channel from hydrostatic effects). The velocities in the microchannel were then determined by tracking the motion of the tracer particles. This was accomplished by epifloures-cent microscopy (Nikon TE-200 inverted microscope equipped with a 100× oil-immersion objective). Images were captured using a cooled charge-coupled device (CCD) camera (IDT 1500-EX, Tallahassee, FL) with 6.45 μm× 6.45 μm pixel resolution and a 12-bit dynamic range with 1×1 binning, for an effective 64.5 nm×64.5 nm per pixel resolution. 700 pixel×700 pixel images were captured at a rate of 12 Hz. Particle tracking velocimetry (PTV) algorithms were used to generate velocity fields, from which average and fluctuation statistics, as well as temporal and spatial correlations, were computed and analyzed.

Computation of the spatial correlation function: The normalized spatial correlation function is defined as:

$$\Omega(r) = \frac{\left\langle \vec{u}_1(\vec{r}_1) \right\rangle \cdot \left\langle \vec{u}_2(\vec{r}_2) \right\rangle}{\left\langle \vec{u}(\vec{r}) \cdot \vec{u}(\vec{r}) \right\rangle} \quad (3)$$

where $\vec{u}$ is a unit vector and the angle brackets denote an ensemble average over all vectors and all time t_i, ($i = 1 \ldots N$). The correlation is normalized so that at zero separation it has a value of one. In practice, we group the spatial vector into "shells" that encompass a range of particle separations, $r_2 - r_1|$. For simplicity, we have not taken into account the orientation of the particle separation with respect to the pumping direction, although this might prove important. The correlations were not computed for small particle separations, $r < 2.5$ μm, as it is likely that there are hydrodynamic interactions between particles[37,38] at this range.

Acknowledgements

This work was supported by the DARPA BioMotors program and the Ostrach Graduate Fellowship (M.J.K.). The assistance of and collaboration with Howard Berg, Linda Turner, Nicholas Darnton, Thomas Powers, Greg Huber, and MunJu Kim are most gratefully acknowledged.

[1] M. A. Unger, H.-P. Chou, T. Thorsen, A. Scherer, S. Quake, *Science* **2000**, *288*, 113–116.
[2] C. Chen, J. Santiago, *J. Microelectromech. Syst.* **2002**, *11*, 672–683.
[3] S. Qian, J. Zhu, H. H. Bau, *Phys. Fluids* **2003**, *14*, 3584–3592.
[4] H. Noji, Y. Ryohei, M. Yoshida, K. Kinosita, *Nature* **1997**, *386*, 299–302.
[5] R. K. Soong, G. D. Bachand, H. P. Neves, A. G. Olkhovets, H. G. Craighead, C. D. Montemagno, *Science* **2000**, *290*, 1555–1558.
[6] Y. Hiratsuka, T. Tada, K. Oiwa, T. Kanayama, T. Q. P. Uyeda, *Biophys. J.* **2001**, *81*, 1555–1561.
[7] H. Hess, G. D. Bachand, V. Viola, *Chem. Eur. J.* **2004**, *10*, 2110–2116.
[8] D. B. Weibel, P. Garstecki, D. Ryan, W. R. DiLuzio, M. Mayer, J. E. Seto, G. M. Whitesides, *Proc. Natl. Acad. Sci. USA* **2005**, *102*, 11 963–11 967.
[9] Y. Hiratsuka, M. Miyata, T. Tada, T. Q. P. Uyeda, *Proc. Natl. Acad. Sci. USA* **2006**, *103*, 13 618–13 623.
[10] H. C. Berg, in *E.coli in Motion*, Springer Verlag, New York **2003**, pp. 42–83.
[11] M. J. Kim, J. C. Bird, A. J. Van Parys, K. S. Breuer, T. R. Powers, *Proc. Natl. Acad. Sci. USA* **2003**, *100*, 15 481–15 485.
[12] X. L. Wu, A. Libchaber, *Phys. Rev. Lett.* **2000**, *84*, 3017–3020.
[13] M. J. Kim, K. S. Breuer, *Phys. Fluids* **2004**, *16*, 78–81.
[14] M. J. Kim, K. S. Breuer, *Anal. Chem.* **2007**, *79*, 955–959.
[15] N. Darnton, L. Turner, K. S. Breuer, H. Berg, *Biophys. J.* **2004**, *86*, 1863–1870.
[16] M. J. Kim, K. S. Breuer, *J. Fluids Eng.* **2007**, *129*, 319–324.
[17] B. Behkam, M. Sitti, *Appl. Phys. Lett.* **2007**, *90*, 023 902.
[18] M. D. Manson, P. Tedesco, H. C. Berg, F. M. Harold, C. van der Drift, *Proc. Natl. Acad. Sci. USA* **1977**, *74*, 3060–3064.
[19] D. Duffy, C. McDonald, O. Schueller, G. M. Whitesides, *Anal. Chem.* **1998**, *70*, 4974–4984.
[20] S. M. Block, H. C. Berg, *Nature* **1984**, *309*, 470–472.
[21] S. Devasenathipathy, J. G. Santiago, *Anal. Chem.* **2002**, *74*, 3704–3713.
[22] M. J. Kim, A. Beskok, K. D. Kihm, *Exp. Fluids* **2002**, *33*, 170–180.
[23] J. P. Brody, P. Yager, R. E. Goldstein, R. H. Austin, *Biophys. J.* **1996**, *71*, 3430–3441.
[24] H. C. Berg, in *Random Walks in Biology*, Princeton University Press, Princeton, NJ **1993**, pp. 12–49.
[25] D. F. Blair, *Nanotechnology* **1991**, *2*, 123–133.
[26] H. C. Berg, L. Turner, *Biophys. J.* **1990**, *58*, 919–930.
[27] Z. Liu, K. D. Papadopoulos, *Appl. Environ. Microbiol.* **1995**, *61*, 3567–3572.
[28] L. Turner, W. S. Ryu, H. C. Berg, *J. Bacteriol.* **2000**, *182*, 2793–2801.
[29] H. C. Berg, D. A. Brown, *Nature* **1972**, *239*, 500–504.
[30] Y. Q. Cui, R. G. J. M. van der Lans, K. C. A. M. Luyben, *J. Bacteriol.* **2000**, *57*, 409–419.
[31] M. B. Short, C. A. Solari, S. Ganguly, T. R. Powers, J. O. Kessler, R. E. Goldstein, *Proc. Natl. Acad. Sci. USA* **2006**, *103*, 8315–8319.
[32] H. C. Berg, *Annu. Rev. Biochem.* **2003**, *72*, 19–54.
[33] H. C. Berg, L. Turner, *Biophys. J.* **1990**, *58*, 919–930.

[34] K. Maeda, Y. Imae, J. I. Shioi, F. Oosawa, *J. Bacteriol.* **1976**, *127*, 1039–1046.
[35] R. M. Macnab, D. E. Koshland, *Proc. Natl. Acad. Sci. USA* **1972**, *69*, 2509–2512.
[36] E. Steager, C.-B. Kim, J. Patel, S. Bith, C. Naik, L. Reber, M. J. Kim, *Appl. Phys. Lett.* **2007**, *90*, 263 901.
[37] W. B. Russel, D. A. Saville, W. R. Schowalter, in *Collodial Dispersions*, InterScience, New York **1989**, pp. 103–177.
[38] J. C. Crocker, *J. Chem. Phys.* **1997**, *106*, 2837–2840.

Received: August 3, 2007
Published online on December 18, 2007